Pillar-induced droplet merging in microfluidic circuits†‡

Xize Niu,[a,b] Shelly Gulati,[a,b] Joshua B. Edel*[a,b] and Andrew J. deMello*[a]

Received 1st August 2008, Accepted 8th September 2008
First published as an Advance Article on the web 8th October 2008
DOI: 10.1039/b813325e

A novel method is presented for controllably merging aqueous microdroplets within segmented flow microfluidic devices. Our approach involves exploiting the difference in hydrodynamic resistance of the continuous phase and the surface tension of the discrete phase through the use of passive structures contained within a microfluidic channel. Rows of pillars separated by distances smaller than the representative droplet dimension are installed within the fluidic network and define passive merging elements or chambers. Initial experiments demonstrate that such a merging element can controllably adjust the distance between adjacent droplets. In a typical scenario, a droplet will enter the chamber, slow down and stop. It will wait and then merge with the succeeding droplets until the surface tension is overwhelmed by the hydraulic pressure. We show that such a merging process is independent of the inter-droplet separation but rather dependent on the droplet size. Moreover, the number of droplets that can be merged at any time is also dependent on the mass flow rate and volume ratio between the droplets and the merging chamber. Finally, we note that the merging of droplet interfaces occurs within both compressing and the decompressing regimes.

Introduction

Over the last decade microfluidic systems have developed into valuable instrumental platforms for performing high-throughput chemistry and biology.[1] More recently microfluidic systems that utilize flow instabilities between immiscible fluids to generate suspended droplets have attracted particular attention.[2] In such systems, droplets are made to spontaneously form when laminar streams of aqueous reagents are injected into an immiscible carrier fluid, either at a T junction[3] or in flow focusing geometry.[4] Either approach allows monodisperse, picoliter droplets of variable composition to be generated at kHz frequencies.[5]

The ability to controllably merge droplets within segmented flow systems is of high importance when performing complex chemical or biological analyses.[6] Unfortunately, the controlled merging of multiple droplets in a sequential fashion is not straightforward. Although the emulsions produced in microfluidic systems are thermodynamically metastable, the process of merging (in effect the reverse of generation) is usually not predictable, due to subtle variations in interfacial tension, surface topography of microchannels, and fluidic properties (such as of droplet size and velocity).[7] As noted, droplet merging is essential in many applications including sequential reactions;[8] multiple step manipulation of cells[9] or high-throughput bioassays.[10] Furthermore, the ability to merge and split droplets or bubbles in a high throughput manner will significantly impact the use of bubble logic systems for exchanging chemical and electronic information.[11] In all of the above merging processes, it is noted that large time and spatial scales are involved. For example, timescales may range from the sub-microsecond regime for some chemical reactions to many hours and even days for cell-based assays. Similarly, large spatial scales also exist within the two key merging processes (*i.e.* droplets must approach each other before the component interfaces interact to drive the merging process).

Several techniques have been developed to merge droplets. These are either active and involve components such as electric fields,[12,13] or passive and utilize the surface properties[14] or structure[15] of the fluidic conduit. In the current paper we focus on passive droplet merging due to the simplicity of device fabrication and operation. To date, most examples of droplet merging have incorporated channel expansions that facilitate the depletion of the continuous phase between adjacent droplets.[15,16] Unfortunately, expansions of this type may also increase droplet freedom, allowing motion paths to be disturbed, and thus reducing control over the merging process.

In this paper, we report on a new approach for passively merging droplets in a controlled manner. Significant advantages of our approach include the capacity to adjust the inter-droplet distance in a facile manner and the ability to selectively merge droplets according to their size or number. Fig. 1(a) illustrates the basic structure of the microfluidic merging element. Droplets generated upstream are directed into a single channel *via* a y-junction. Within the merging element, the channel is made wider than the input channel and installed with an array of pillar elements. Previously pillars of this kind have been used

[a]*Department of Chemistry, Imperial College London, Exhibition Road, South Kensington, London, UK SW7 2AZ. E-mail: a.demello@imperial.ac.uk, joshua.edel@imperial.ac.uk*
[b]*Institute of Biomedical Engineering, Imperial College London, Exhibition Road, South Kensington, London, UK SW7 2AZ*

† In honour of Andreas Manz on his retirement as Chair of the *Lab on a Chip* Editorial Board.

‡ Electronic supplementary information (ESI) available: Movies 1–3. See DOI: 10.1039/b813325e

to control molecular mixing or separation within microfluidic structures.[17–19] In our design, the pillars divide the entire merging element into three channels; two side branches (of width W_1 and W_3) and a middle branch (where the width W_2 reduces as a function of distance through the pillar array). These three channels are interconnected *via* side channels (of width W_s) between individual pillars. The magnitude of W_s is designed to be smaller than both W_2 and the representative droplet diameter, to ensure that the droplets will neither go through the side channels as a whole nor breakup into sister droplets due to the side channels.[20] Accordingly, droplets entering the merging chamber will be localised in the middle branch, whilst the continuous phase is able to flow through all three parallel branches. In a sense, the pillars act as a filter, but also allow for all of the continuous phase to flow back into the main channel at the end of the merging element. Moreover, such a 'single input' and 'single output' merging chamber ensures a constant total fluidic mass between the inlet and outlet, and thus allows the merging element to be installed in any location within the microfluidic network, without inducing asymmetries in mass and pressure distribution.

Experimental

In the current studies, microfluidic device were fabricated in polydimethylsiloxane (PDMS) using standard soft lithographic technique.[21] As shown in Fig. 1(b), pillars are designed to be the same height as the input channel, thus necessitating only a single lithographic step in the fabrication process. Specifically, to form the structured PDMS layer, PDMS base and curing agent (Sylgard 184; Dow Corning) were mixed in a ratio of 10 : 1 w/w, degassed and decanted onto an SU-8 master. The resulting structure was cured for 2 h in an oven at 65 °C. After thermal curing the polymer layer was pealed off the master and inlet and outlet holes punched through the structured PDMS layer. This layer is then contacted with a flat PDMS layer coated on a thin glass substrate and baked at 80 °C for 4 h to form the completed microdevice.

The fluidic channels have a rectangular cross section of 50 × 50 μm and dilate to a width of 250 μm to form the merging element. The pillar array contains pillars having a square cross section of 20 μm and a pitch of 40 μm (with $W_s = 20$ μm). In initial experiments hexadecane (Sigma) was used as the continuous phase. Furthermore, it should be noted that no additional surfactant was added to the system. Deionised water or deionised water containing a small amount of food dye were used as the discrete phase. The interfacial tension for the entire system was measured to be approximately 50 mN m^{-1}. Precision syringe pumps (PHD 2000, Harvard Apparatus) were used to motivate fluids at volumetric flow rates ranging between 2.5 and 26.5 μl min^{-1}. A high speed camera (Phantom®, v649) was used for data acquisition and Matlab® was used to analyse and process recorded images.

Results and discussion

Fig. 1(c) shows a large-scale view of the microfluidic device during operation (see also ESI Movie 1‡). During initial calibration, 100 μm diameter droplets were generated using a flow focusing channel, and an oil-to-water ratio of 3 : 1. Additionally, a secondary oil inlet was used, after the droplet generation, to adjust the distance between droplets (visible in the top right hand part of Fig. 1(c)). Inspection of both Fig. 1(c) and Movie 1‡ demonstrates that the merging element is highly efficient at combining neighbouring input droplets to form a droplet twice as large. The merging process is extremely stable, and has been operated continually for periods in excess of several hours each round in different experiments.

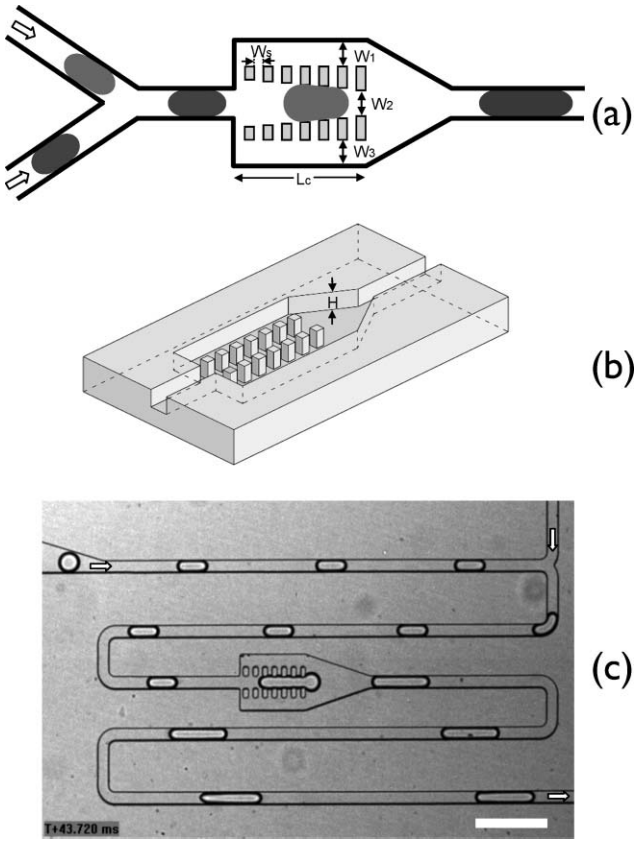

Fig. 1 (a) Schematic illustration of the microfluidic merging element. Two channel branches are connected by a Y junction. The merging chamber is 250 um in width and divided into three branches by two rows of pillars. (b) Three-dimensional illustration showing the top PDMS layer with all channel and pillars having the same depth and height. (c) CCD image showing the merging of two droplets. Scale bar: 300 μm.

Fig. 2(a) provides a more detailed analysis of the merging process. The first drop (marked D_1) enters the merging chamber, decelerates to a standstill, and effectively 'waits' for a subsequent drop (marked D_2) to enter the middle branch. The head of D_2 then pushes the tail of D_1 (at ~ 25 ms) to initiate forward motion. During this movement, the interfaces between the two droplets are disturbed *via* drop deformation and merging occurs. Fig. 2(b) and (c) provide an analysis of the individual and merged droplet velocities and the inter-droplet separation as a function of time.

Through variation of the input volumetric flow rates, input inter-droplet separations were varied from tens of microns to tens of millimetres. Such a variation had no detectable affect on the droplet merging mechanism. Indeed, the first droplet (D_1) is able to wait in the middle branch of the merging chamber for

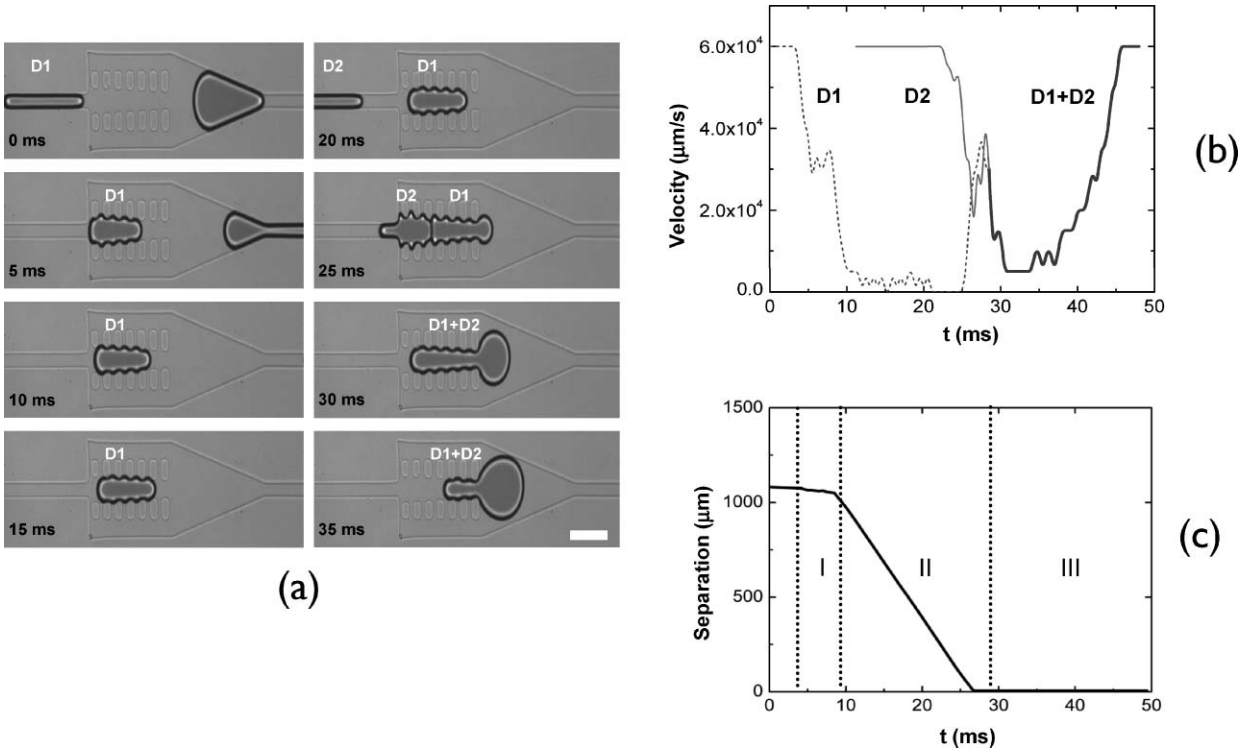

Fig. 2 (a) Sequence of images demonstrating the merging of two adjacent droplets. The first droplet (marked D1) merges with the second (marked D2). The velocity and separation of D1 and D2 during the merging process (a) are plotted in (b) and (c) as a function of time. In (b), velocity is measured with respect to the head of both droplets. In (c), separation is defined as the distance between the tail of D1 and the head of D2. The merging process can be divided into three parts: (I) the deceleration of D1, (II) the period that D1 is stationary and finally (III), the movement of the merged droplet out of the middle branch. Scale bar: 100 μm.

many hours if the water inlet flow is terminated. Accordingly, such a merging chamber can endure large spatial variations.

The physical processes underlying this observed merging can be described by considering a two-step competition between hydrodynamics forces and surface tension. The first aspect of this competition occurs at the start of the middle branch, with the second occurring at the end of the middle branch. Before entering the merging chamber, the input droplets move at an almost constant velocity within the oil, and only weak corner-flows exist. Once a droplet enters the merging chamber, and because W_2 is larger than W_s, surface tension will keep the droplet within the middle branch, while the average flow velocity decreases due to the channel expansion. Such an expansion, combined with the hydrodynamic resistance[22] of the droplets acts to generate an uneven droplet acceleration as shown in Fig. 2(b). Moreover, the deformation of the droplet, due to the non-uniform magnitude of W_2, generates a differential pressure between the head and the tail of the droplet. At this point the droplet is considered to be quasi-stationary. P_0 defines the hydraulic pressure close to the tail of the droplet, and P_1 defines the pressure close to the head, as illustrated in Fig. 3(a). In this situation, the droplet with radii r_1 and $H/2$ in the tail and radii r_2 and $H/2$ at the head is confined between the pillars and channels walls. Thus, from Laplace's law $P_{droplet} - P_0 = \gamma(1/r_1 + 2/H)$ and $P_{droplet} - P_1 = \gamma(1/r_2 + 2/H)$. Here $P_{droplet}$ is the pressure inside the droplet, γ defines the interfacial tension. Considering $r_2 = r_1 - L\tan\alpha$, as shown in Fig. 3(a), the differential pressure ΔP_d is given by,

$$\Delta P_d = P_0 - P_1 = \gamma L\tan\alpha/(r_1(r_1 - L\tan\alpha)) \quad (1)$$

At the same time, the oil phase flows continuously through the first several pairs of side channels to the side branches. Accordingly, the total pressure drop between the tail and the head of a droplet in the middle branch is a combination of the pressure drop in the side channels (near the tail) and in the side branches, *i.e.*

$$\Delta P_d = 12\mu L_s Q_1/(HW_s^3) + 6\mu QL/(HW_1^3) \quad (2)$$

Here W_1 and W_3 are considered to be equal. Q defines the total flow rate and Q_1 defines the average flow rate in one side channel. Thus $Q_1 \approx Q/n$, where n is the total number of side channels between the drop tail and the entrance of the merging chamber. In addition, L_s defines the length of the side channel and μ is the dynamic fluid viscosity. The first part of the right hand side of eqn (2) results from the pressure drop at the side channel near the droplet tail, while the second part results from the pressure drop in the side branch. Now, if n is small, and $\Delta P > \Delta P_d$, the droplet will be pushed forward. This will cause a decrease in ΔP due to the involvement of more side channels. Eventually a balance is reached when $\Delta P \leq \Delta P_d$, and the droplet will stop.

The second component of the competition between hydrodynamics forces and surface tension occurs at the end of the merging chamber. When the head of a droplet is pushed out of the middle branch, it deforms towards a more rounded shape due to interfacial tension, and then 'drags' out the remainder of

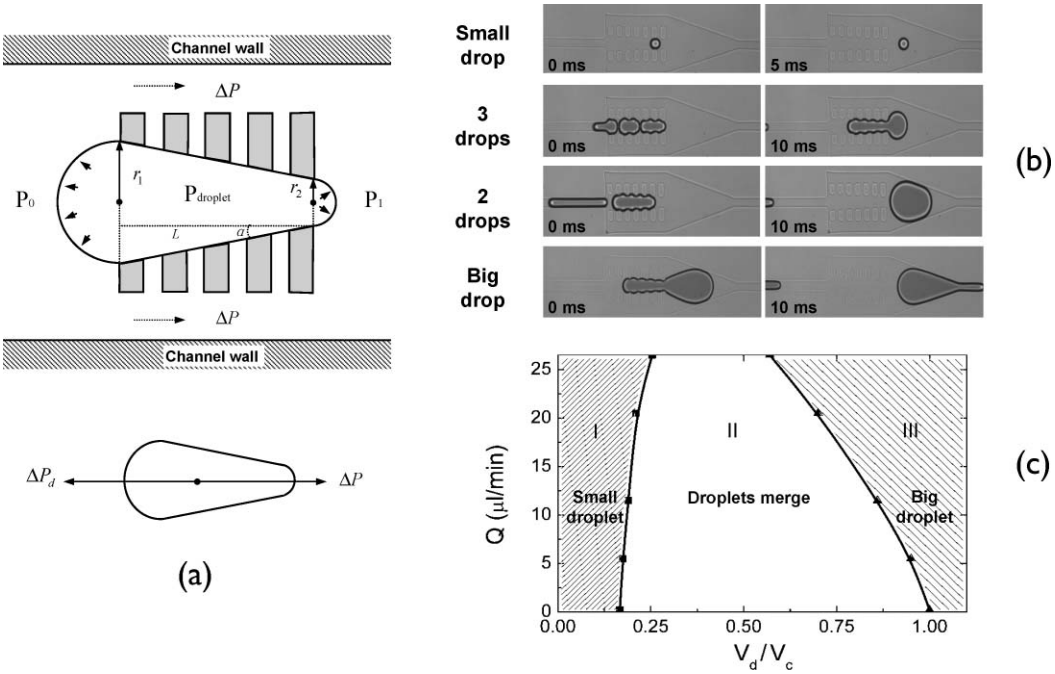

Fig. 3 (a) Schematic analysis of force balance when a droplet is trapped in the attenuated merging chamber. (b) Snapshots of small (the radius of the droplet is less than W_2), medium and large (the volume of the droplet V_d is bigger than the volume of the middle branch V_c) droplets transiting the merging element. (c) Stability diagram correlating the volume ratio V_d/V_c with the volumetric flow rate. In region I no droplet merging occurs, in region II between 2 and 5 droplets will merge depending on the flow conditions, and in region III no droplet merging occurs.

the droplet from the middle branch. This process is illustrated at 30 and 35 ms in Fig. 2(a). Such a drag force accelerates the movement of the droplet tail, and ensures that a specific number of droplets can be merged. Indeed, the merged droplet maintains its integrity in the wider part of the merging chamber, without being further sheared into smaller droplets by side branch flows.

The balance between ΔP_d and ΔP directly implies a scaling law for this merging process. For a small droplet having a diameter smaller than W_2, the differential pressure due to surface tension is negligible. For this reason, the droplet can move along the middle branch, without perturbation, as shown in Fig. 3(b). If the droplet diameter exceeds W_2, ΔP_d comes into effect and the droplet can slow down and stop in the middle branch. The number of droplets that can be stopped depends sensitively on the ratio of the total droplet volume V_d to the chamber volume V_c. Therefore, control of the merging chamber length or the droplet size, allows merging of the desired number of droplets. Fig. 3(b) shows snapshots of merging events for 3 and 2 droplets (see also ESI Movie 2‡). We also achieved stable merging of both 4 and 5 droplets. However, it must be noted that if $V_d > V_c$, the droplet can completely block the continuous flow from the side channels and the force balance between ΔP_d and ΔP becomes invalid. In this situation, the droplet will pass thorough the merging chamber without stopping.

A parametric study was performed by adjusting the ratio V_d/V_c, and mass flow rate Q. The results of this study are summarised in Fig. 3(c). The parametric space is divided into three areas according to the droplet size, as analyzed above. It can be seen that as Q increases more side channels are needed to decrease ΔP and therefore the total volume of droplets that can be merged in the chamber becomes smaller.

Since the merging chamber can confine a droplet in a designated position it is comparatively easy to study the detailed break up of component interfaces during merging.[23] Fig. 4 shows that for the oil–water system used, merging occurs within both *decompressing* (Fig. 4(a)) and *compressing* regimes (Fig. 4(b)). Here we define a decompressing regime to be one in which adjacent droplets are firstly compressed and then separated (due to the channel geometry). Droplet merging is favoured during this separation period.[16] Such a *decompressing* regime is clearly shown in Fig. 4(a). We observe that small droplets usually undergo such a decompression during merging. Conversely, larger droplets can merge directly during a compression process as shown in Fig. 4(b). Although direct observation of the drainage of the oil film between the droplets on the nanoscale has yet to be reported, it is postulated that merging occurs when the oil film is depleted below a certain thickness. Eqn (2) indicates that the differential pressure increases for larger droplets (with bigger L). Accordingly, the depletion of the interfacial oil film is faster for bigger droplets, which is consistent with the observations in Fig. 4(a) and (b).

Moreover, it is observed that merging can happen in less than 40 μs, and that efficient mixing of droplet contents can occur rapidly. This can be seen in Fig. 4(c) where two droplets of similar size are mixed over a 7 ms period. The images in Fig. 4(c) (and ESI Movie 3‡) also show that the mixing in the droplet is laminar and convection driven. Hence the mixing time is proportional to the time the droplet passes through the merging chamber.

In conclusion, using the concept of geometrically mediated merging of droplets, we have demonstrated selective and controllable droplet coalescence within a microfluidic system. We believe that such a merging element will find application in many

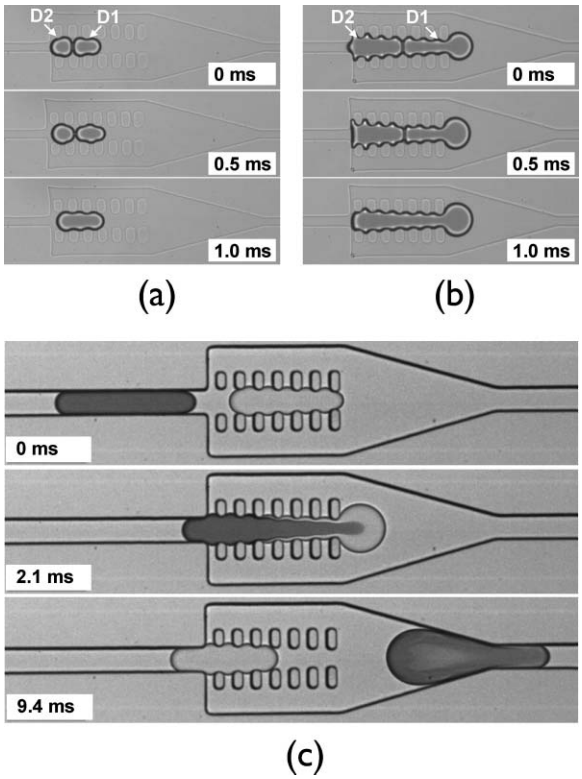

Fig. 4 (a) Illustration of a decompressive merging of two droplets with radii similar to the width of the chamber. At $t = 0$, D2 contacts D1. After overcoming the pressure band gap due to interfacial tension, D1 accelerates to settle into a wider region and takes on a more rounded shape. In this decompressing process, the interfaces between the two droplets break up. (b) Illustration of a compressive merging of two larger droplets. Here D2 compresses with D1, after which both droplets advance until the interface breaks up and merging takes place. (c) Merging and mixing of two different droplets having the same size. Complete mixing is achieved when the merged droplet moves out of the merging element (~7 ms after entering the merging element).

areas of chemical and biological processing, including complex biological assays and small molecule synthesis and screening. We also note that since droplets can be made to stay in our merging chamber for extended periods of time, the element provides a simple platform for droplet trapping, and thus application in cell-based analysis systems.

Acknowledgements

This work was supported by the RCUK Basic Technology Programme. XZ would also like to thank Professor Ping Sheng and Weijia Wen from The Hong Kong University of Science and Technology for useful discussions.

References

1 A. J. deMello, *Nature*, 2006, **442**, 394.
2 B. Zheng and R. F. Ismagilov, *Angew. Chem., Int. Ed.*, 2005, **44**, 2520.
3 T. Thorsen, R. W. Roberts, F. H. Arnold and S. R. Quake, *Phys. Rev. Lett.*, 2001, **86**, 4163.
4 S. L. Anna, N. Bontoux and H. A. Stone, *Appl. Phys. Lett.*, 2003, **82**, 364.
5 D. R. Link, S. L. Anna, D. A. Weitz and H. A. Stone, *Phys. Rev. Lett.*, 2004, **92**, 054503.
6 I. Shestopalov, J. D. Tice and R. F. Ismagilov, *Lab Chip*, 2004, **4**, 316.
7 M. J. Fuerstman, P. Garstecki and G. M. Whitesides, *Science*, 2007, **315**, 828.
8 S. J. Kim, Y.-A. Song, P. L. Skipper and J. Han, *Anal. Chem.*, 2006, **78**, 8011.
9 M. Y. He, J. S. Edgar, G. D. M. Jeffries, R. M. Lorenz, J. P. Shelby and D. T. Chiu, *Anal. Chem.*, 2005, **77**, 1539.
10 M. Srisa-Art, A. J. deMello and J. B. Edel, *Anal. Chem.*, 2007, **79**, 6682.
11 M. Prakash and N. Gershenfeld, *Science*, 2007, **315**, 832.
12 C. Priest, S. Herminghaus and R. Seemann, *Appl. Phys. Lett.*, 2006, **89**, 134101.
13 K. Ahn, J. Agresti, H. Chong, M. M. Marquez and D. A. Weitz, *Appl. Phys. Lett.*, 2006, **88**, 264105.
14 L. M. Fidalgo, C. Abell and W. T. S. Huck, *Lab Chip*, 2007, **7**, 984.
15 Y.-C. Tan, J. S. Fisher, A. I. Lee, V. Cristini and A. P. Lee, *Lab Chip*, 2004, **4**, 292.
16 N. Bremond, A. R. Thiam and J. Bibette, *Phys. Rev. Lett.*, 2008, **100**, 024501.
17 L. R. Huang, E. C. Cox, R. H. Austin and J. C. Sturm, *Science*, 2004, **304**, 987.
18 X. Z. Niu, L. Y. Liu, W. Wen and P. Sheng, *Phys. Rev. Lett.*, 2006, **97**, 044501.
19 A. Gunther, M. Jhunjhunwala, M. Thalmann, M. A. Schmidt and K. F. Jensen, *Langmuir*, 2005, **21**, 1547.
20 L. Ménétrier-Deremble and P. Tabeling, *Phys. Rev. E*, 2006, **74**, 035303.
21 Y. Xia and G. M. Whitesides, *Angew. Chem., Int. Ed.*, 1998, **37**, 550.
22 M. J. Fuerstman, A. Lai, M. E. Thurlow, S. S. Shevkoplyas, H. A. Stone and G. M. Whitesides, *Lab Chip*, 2007, **7**, 1479.
23 N. H. Chen, T. Kuhl, R. Tadmor and Q. Lin, *Phys. Rev. Lett.*, 2004, **92**, 024501.